Nano Energy 128 (2024) 109879

Contents lists available at ScienceDirect

Nano Energy

journal homepage: www.elsevier.com/locate/nanoen

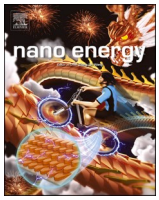

Solar-driven hydrogen production based on moisture adsorption-desorption cycle

Lu Huang [a,c,d,1], Peng Liu [a,c,1], Chenglong Qin [a,c,d], Chengxiang Gui [a,c,d], Xiantao Zhang [a,c,d], Tingting Ren [a,c,d], Yanlin Ge [a,c,d], Yingni Yu [a,c,d], Zhichun Liu [b,*], Lingen Chen [a,c,d,**]

[a] Institute of Thermal Science and Power Engineering, Wuhan Institute of Technology, Wuhan 430205, China
[b] School of Energy and Power Engineering, Huazhong University of Science and Technology, Wuhan, Hubei 430074, China
[c] Hubei Provincial Engineering Technology Research Center of Green Chemical Equipment, Wuhan 430205, China
[d] School of Mechanical & Electrical Engineering, Wuhan Institute of Technology, Wuhan, Hubei 430205, China

ARTICLE INFO

Keywords:
Photocatalytic hydrogen evolution
Interfacial photocatalysis
Water vapor splitting
Atmospheric water harvesting
Hygroscopic hydrogel
Self-regeneration

ABSTRACT

Photocatalytic hydrogen production by water splitting is considered one of the most promising green hydrogen manufacturing technologies, but the actual outdoor deployment of this technology is limited by the availability of water feedstocks in geographical locations. An integrated device consisting of a photocatalytic layer and an atmospheric water harvesting material that can achieve in-situ photocatalytic water vapor splitting for hydrogen production by spontaneously capturing moisture from the air as a water feedstock is proposed herein. The integrated system has excellent photocatalytic and photothermal synergistic ability, low hydrogen diffusion resistance by interfacial photocatalysis, and high stability by isolating salts contamination. The system can achieve a hydrogen production rate of 425.4 μmol g^{-1} h^{-1} and a water vapor supply rate of 0.121 kg m^{-2} h^{-1} under one sun illumination, and has a water vapor adsorption rate of 0.03 kg m^{-2} h^{-1} under dark conditions in the laboratory. Furthermore, this hybrid device obtains a total hydrogen production of up to 3963.1 μmol g^{-1} in the real outdoor daytime and accomplishes water regeneration within 10 hours by capturing environmental moisture at night. This work provides a suitable solution for hydrogen production in areas with water scarcity or drought.

1. Introduction

As an effective substitute for traditional carbon-based fossil energy, hydrogen (H_2) energy is an ideal fuel to reduce carbon emissions and environmental pollution[1–3]. Solar-driven hydrogen evolution by water splitting is a very promising green hydrogen production method, which has been widely favored [4–6]. Compared with photoelectrochemical cells [7] and photovoltaic-assisted electrolyzers [8], photocatalytic hydrogen evolution (PHE) technology has obvious advantages such as system simplification, cost-effectiveness, and high safety [9–11]. In the past period of time, extensive efforts have been made to improve the performance of photocatalysts materials through band gap engineering [12], heterostructure design [13], dual-cocatalysts construction [14] for enhancing the conversion efficiency of solar to hydrogen (STH) [15]. Although the STH efficiency of PHE systems has recently exceeded 9 % [16], the actual outdoor deployment of PHE systems is still restricted by geographical availability of water feedstocks. In order to overcome the limitation of using pure water as raw materials in traditional PHE systems, recent researchers have tended to develop systems that use untreated water feedstocks such as seawater or industrial wastewater to drive the photocatalytic water splitting process [17–19], but few studies have focused on the operation of PHE systems in areas without access to liquid water sources.

Atmospheric water, as a ubiquitous natural water source [20] and accounting for about 10 % of the freshwater resources on the earth's surface [21], provides a promising opportunity to capture moisture from the ambient air [22–24]. Atmospheric water harvesting (AWH) is regarded as an effective method for supplementing freshwater resources in water-stressed or arid regions [25–27], which can provide an effective avenue to achieve sustainable water supply for water-deficient PHE

* Corresponding author.
** Corresponding author at: Institute of Thermal Science and Power Engineering, Wuhan Institute of Technology, Wuhan 430205, China.
E-mail addresses: zcliu@hust.edu.cn (Z. Liu), lingenchen@hotmail.com (L. Chen).
[1] These authors contributed equally to this work.

https://doi.org/10.1016/j.nanoen.2024.109879
Received 21 March 2024; Received in revised form 25 May 2024; Accepted 8 June 2024
Available online 10 June 2024

systems. Typically, sorption-based AWH can use various hygroscopic materials (e.g., metal-organic frameworks (MOFs) [28–30], zeolites [31], and porous hydrogels with hygroscopic salts [32–34]) to spontaneously adsorb water molecules from the air and release water vapor driven by solar-thermal energy [35–37]. Furthermore, in most PHE systems, only high-energy photons in the ultraviolet band of sunlight can drive the water splitting reaction, and a large number of visible and infrared band photons are absorbed and not utilized, which will be an ideal energy source to drive the desorption process of sorption-based AWH system for producing water vapor. Moreover, photocatalytic water splitting by gas-phase water vapor has been verified to have lower energy requirements because gaseous water has a lower Gibbs free energy, while water vapor without any impurities can maintain the long-term activity and lifetime of the photocatalyst [38–40]. Hence, solar-driven AWH coupled with a PHE system may break through the technical bottleneck that the current PHE system cannot work in rural, desert and arid areas with abundant solar energy and ubiquitous moisture.

To address the geographical limitations of the water supply chain in the PHE system, this article will propose an integrated AWH-PHE device that can obtain water feedstocks from moisture in the environment and provide water vapor to photocatalysts for H_2 production without additional energy consumption except for solar energy. The hybrid system consists of a top Pt-TiO_2/PTFE sheet acts as a photocatalytic layer to split water vapor from the AWH module to generate H_2 and a bottom $CaCl_2$-PAAm hygroscopic hydrogel under the photocatalytic layer serves as a AWH material to capture the ambient moisture. The Pt-TiO_2/PTFE sheet can fully harness the entire solar spectrum that breaks down water vapor to generate H_2 through absorbed ultraviolet light and generates heat through absorbed visible and infrared light to drive the bottom hydrogel to release water vapor in the daytime. The $CaCl_2$-PAAm hygroscopic hydrogel can spontaneously absorb water vapor from the surrounding environment through breathable Pt-TiO_2/PTFE membrane to realize self-regeneration at night. The solar-driven AWH-PHE device will be demonstrated to produce H_2 by using moisture from the air under both laboratory and real outdoor environments. This work will provide a promising route to produce green H_2 fuel using solar energy and atmospheric moisture anywhere.

2. Results

2.1. Design concept of the hybrid AWH-PHE device

Solar energy and moisture are ubiquitous on Earth, even in remote arid or desert regions. A moisture harvesting strategy is designed to provide water vapor for in situ photocatalytic hydrogen production by attaching the PHE module to the top surface of the AWH module. Among them, the PHE module is mainly composed of Pt-TiO_2 photocatalyst and porous PTFE hydrophobic membrane, and the photocatalyst is uniformly attached to the surface of the hydrophobic PTFE membrane by vacuum filtration. The AWH module is mainly composed of a $CaCl_2$-PAAm hygroscopic hydrogel and acrylic mould, and the hygroscopic hydrogel is formed by ultraviolet photopolymerization in the acrylic mould.

Fig. 1 shows the basic working principle of the hybrid AWH-PHE device. During the daytime, the sunlight is absorbed by the Pt-TiO_2/PTFE sheet, where the absorbed low-energy photons in the visible and infrared light bands are mainly converted into heat to drive water evaporation inside the hygroscopic hydrogel to generate water vapor, while the absorbed high-energy photons in the ultraviolet light band decompose the water vapor from the bottom AWH module to produce H_2 on the Pt-TiO_2 catalyst surface. It is worth noting that this

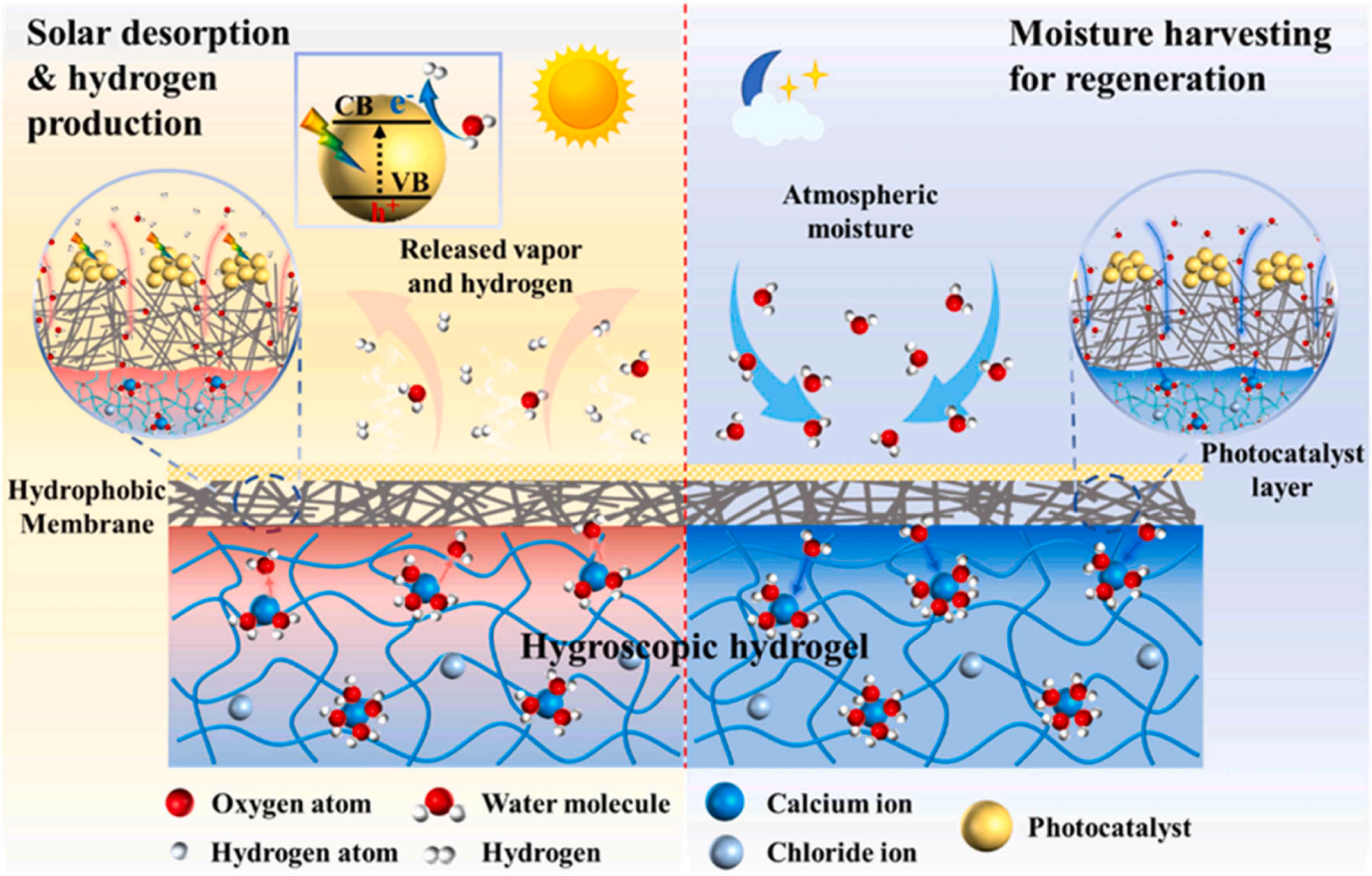

Fig. 1. The working principle of the hybrid AWH-PHE device for capturing moisture from the air to generate H_2 by solar-driven water splitting.

hydrophobic porous PTFE membrane has good hydrophobicity (Fig. S4), which only allows water vapor molecules to pass through, while Ca^{2+} and Cl^- ions inside the hydrogel cannot reach the upper surface of the Pt-TiO_2 catalyst to reduce its catalytic activity. During the night, the hybrid system is opened and exposed to the surrounding atmosphere, and then the water vapor in the air is spontaneously absorbed into the surface of the hygroscopic hydrogel through the upper hydrophobic PTFE membrane because the partial pressure of water vapor in the environment is higher than that of the hygroscopic hydrogel in a dehydrated state. Moreover, the hygroscopic hydrogel has good hydrophilicity and can ensure the rapid transport of water vapor after adsorption (Fig. S5).

2.2. Synthesis and characterization of the photocatalytic material and sorbents

The fabrication process of the Pt-TiO_2/PTFE photocatalytic sheet and the $CaCl_2$-PAAm hygroscopic hydrogel is shown in Fig. 2a. Firstly, Pt-TiO_2 catalyst powders are dispersed by ultrasonic vibration to form a suspension, then it is uniformly attached to the surface of hydrophobic porous PTFE membrane by vacuum filtration, and finally dried to form Pt-TiO_2/PTFE composite membrane as a photocatalytic layer. Acrylamide (AM) monomer precursor with $CaCl_2$ salt is injected into a self-made acrylic mould, and in-situ polymerized in the mould under ultraviolet irradiation to form the $CaCl_2$-PAAm hygroscopic hydrogel. As shown in Fig. S6, the $CaCl_2$-PAAm hydrogel could be stretched up to 2–3 times its original length, which shows that it has sufficient mechanical strength.

The physical photos and corresponding SEM images of the Pt-TiO_2/PTFE composite membrane and the hygroscopic hydrogel are displayed in Fig. 2b. The SEM images of the top Pt-TiO_2/PTFE composite membrane reveal that the PET support layer at the upper surface of PTFE membrane uniformly adhered a layer of Pt-TiO_2 catalyst particles. Meanwhile, the lower surface of PTFE membrane exhibits an obvious interconnected porous network with an average pore diameter of around 0.22 μm. The SEM images of the bottom $CaCl_2$-PAAm hygroscopic hydrogel clearly display its 3D porous structure with a pore diameter of approximately 5–25 μm. These interpenetrating porous networks can provide channels for the rapid water transportation after adsorption and ensure sufficient water storage.

The EDS elemental maps on the surface of PTFE further prove that Pt, Ti, and O elements are uniformly distributed on its surface, demonstrating that there are a large amount of catalysts on the surface of hydrophobic membrane which could be used for photocatalytic reactions (Fig. 2c). The absorption rate of Pt-TiO_2/PTFE composite membrane in the whole solar spectrum band from 300 to 2500 nm is as high as 80.8 % (weighted by AM 1.5 G), indicating that the membrane has good photocatalytic-photothermal effect (Fig. 2d). Fig. 2e shows the temperature distribution of the integrated AWH-PHE device after 15 minutes of irradiation under one sun. It can be seen that the maximum temperature region is concentrated on the surface of the photocatalytic layer and reached up to 45 ℃, which is almost 20 ℃ higher than the ambient temperature. This heat localization phenomenon can effectively improve the water desorption rate from the hygroscopic hydrogel and increase the temperature of photocatalytic water vapor to achieve higher STH conversion efficiency. The long-term limit of water loss for hygroscopic hydrogels of 35 wt% and 45 wt% $CaCl_2$ can reach 2.36 kg m^{-2} and 1.60 kg m^{-2} under one sun for 10 hours, respectively (Fig. S9). This demonstrates that the water content of hygroscopic hydrogels with different $CaCl_2$ concentrations can meet the water supply under long-term high-intensity irradiation.

2.3. Indoor performance test

The H_2 production performance and water harvesting capacity of this integrated AWH-PHE device are first evaluated in the laboratory (Fig. S10). Fig. 3a shows the structural schematic diagram of the measurement system. A solar simulator is used to provide stable solar radiation flux, and the surface temperature and mass changes of the hybrid device are recorded by a K-type thermocouple connected to the acquisition card and an electronic balance, respectively. The amount of H_2 produced by the integrated device is collected by a micro injection needle and injected into the gas chromatograph for quantitative calibration. Fig. 3b shows the comparison of H_2 evolution performance between our proposed interfacial photocatalytic water vapor system and traditional volumetric photocatalysis system under one sun illumination. Due to its higher reaction temperature and lower hydrogen diffusion resistance, the hydrogen evolution rate in interfacial photocatalysis system (425.4 μmol g^{-1} h^{-1}) is 1.43 times higher than that of volumetric photocatalysis system (296.9 μmol g^{-1} h^{-1}). Fig. 3c and Fig. S12 show the effect of Pt loading on hydrogen production rate and water desorption rate. When the Pt loading increases from 1.5 mol% to 6 mol %, the hydrogen production rate first increased and then decreased slightly, while the water desorption rate always increased. This is because the increase of Pt content will improve the solar absorption capacity of the TiO_2 catalysts, and appropriate increase of Pt content can provide more active sites for the activation of water molecules [41].

The content of $CaCl_2$ in hygroscopic hydrogel will affect the water desorption and adsorption rate, thus affecting the hydrogen production performance of the system. As shown in Fig. 3d, when the mass fraction of $CaCl_2$ in the hygroscopic hydrogel increases from 35 % to 45 %, the water desorption rate decreases from 0.121 kg m^{-2} h^{-1} to 0.092 kg m^{-2} h^{-1} under one sun illumination, while the water vapor adsorption rate increases from 0.03 kg m^{-2} h^{-1} to 0.057 kg m^{-2} h^{-1} in dark ambient. This is mainly because as the $CaCl_2$ concentration increases, the evaporation enthalpy and vapor adsorption capacity of water in hydrogel will be improved. Delightedly, the hydrogen production rate of the hygroscopic hydrogel with 50 % $CaCl_2$ mass fraction is only about 25.5 % lower than that of hydrogel with 30 % $CaCl_2$ mass fraction (Fig. S13), so the $CaCl_2$ concentration can be increased to adapt to the environmental conditions in low humidity areas such as deserts or droughts. The hydrogen production and water desorption performance of the hybrid system under 0.8–1.2 sun illumination (i.e., 800 W m^{-2}-1200 W m^{-2}) are then evaluated using a hygroscopic hydrogel with 35 wt% $CaCl_2$. As the solar irradiation flux increases from 0.8 sun to 1.2 sun, the steady-state temperature of the photocatalytic layer in this system increases from 50.43 °C to 63.87 °C (Fig. 3e). These experimental temperature results are consistent with the predicted results of established theoretical model (Fig. 3f and see details in SI-20), and an energy balance analysis of the AWH-PHE system is shown in Fig. S14. Fig. 3g shows the variation of hydrogen production over time under different solar intensities. The hydrogen production rate under 1.2 sun is as high as 506.5 μmol g^{-1} h^{-1}, which is 46.1 % higher than the hydrogen production rate under 0.8 sun (346.7 μmol g^{-1} h^{-1}). This is mainly attributed to higher reaction temperature and vapor concentration, which will accelerate the photocatalytic reaction rate. The increase in solar intensity will enhance the overall hydrogen production rate, which is also predicted through numerical simulation (Fig. 3h). When the 1.5-hour hydrogen production experiment under simulated sunlight is completed, the device is opened and exposed to the same external atmospheric environment for moisture absorption. The moisture absorption regeneration time after irradiation under 0.8 sun, 1 sun, and 1.2 sun were 2.38 h, 5.12 h, and 7.51 h, respectively (Fig. 3i), which indicates the feasibility of using ubiquitous atmospheric water sources to supply the photocatalytic hydrogen production system. Moreover, the hybrid system can also work normally and stably under lower solar intensity of 0.5 sun (Fig. S15).

2.4. Environmental adaptability and durability assessment

In order to assess the environmental adaptability of the AWH-PHE device, the H_2 production performance at different ambient temperatures is tested under one sun illumination (Fig. 4a). The H_2 production rate gradually improves from 332.1 μmol g^{-1} h^{-1} to 609.1 μmol g^{-1} h^{-1}

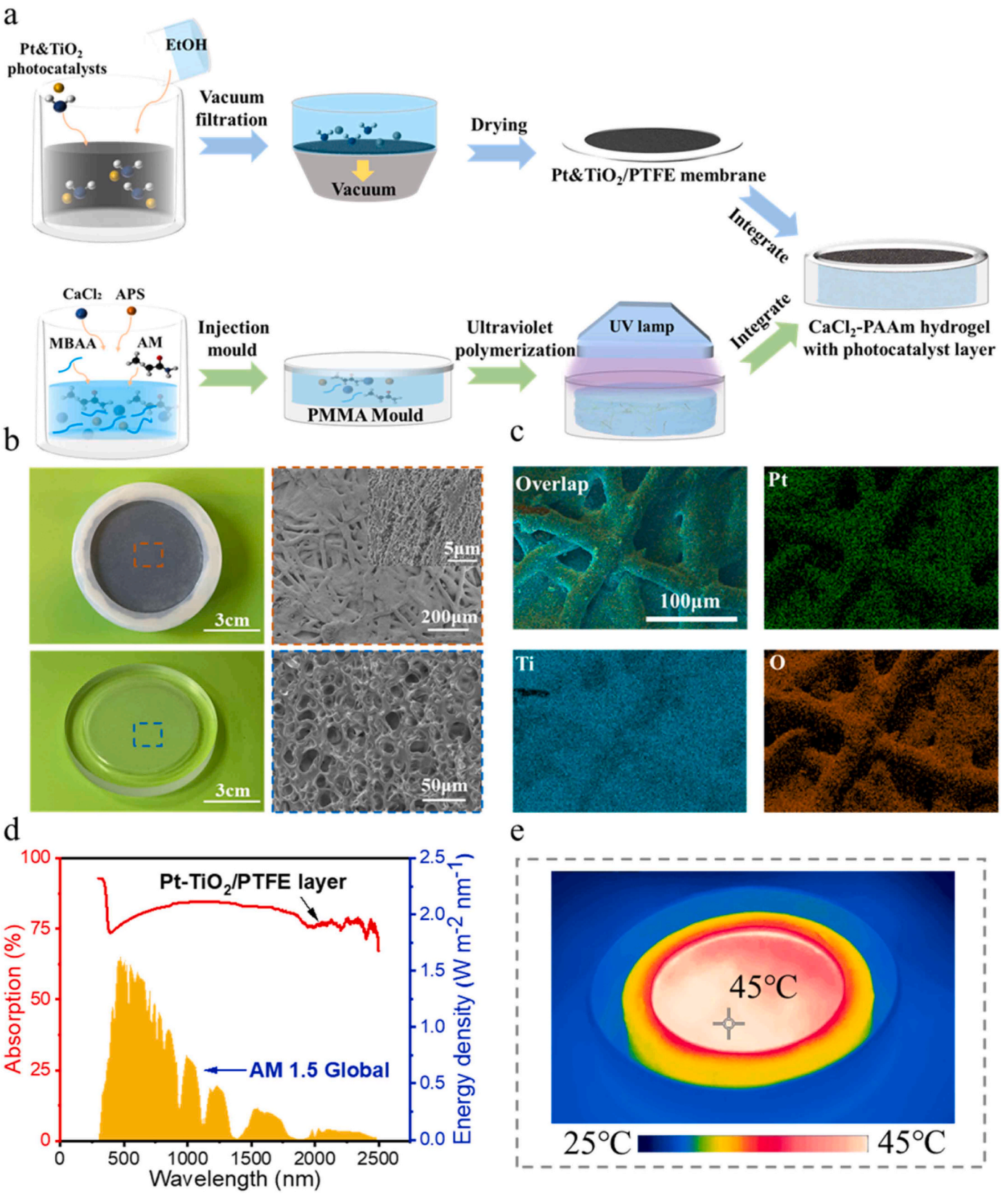

Fig. 2. Synthesis and characterization of the photocatalytic sheet and the sorbent. a, The preparation process of the Pt-TiO_2/PTFE photocatalytic sheet and the $CaCl_2$-PAAm hydrogel sorbent. The photocatalytic sheet is closely attached to the upper surface of the hydrogel sorbent. b, Optical and SEM image of the Pt-TiO_2/PTFE layer and $CaCl_2$-PAAm hydrogel. c, EDS elemental maps of the as-prepared Pt-TiO_2 photocatalyst on the surface of PTFE membrane. d, The absorption spectrum of the photocatalytic layer in the solar wavelength range. e, Infrared thermal imaging from the hybrid AWH-PHE device after 15 minutes of irradiation under one sun.

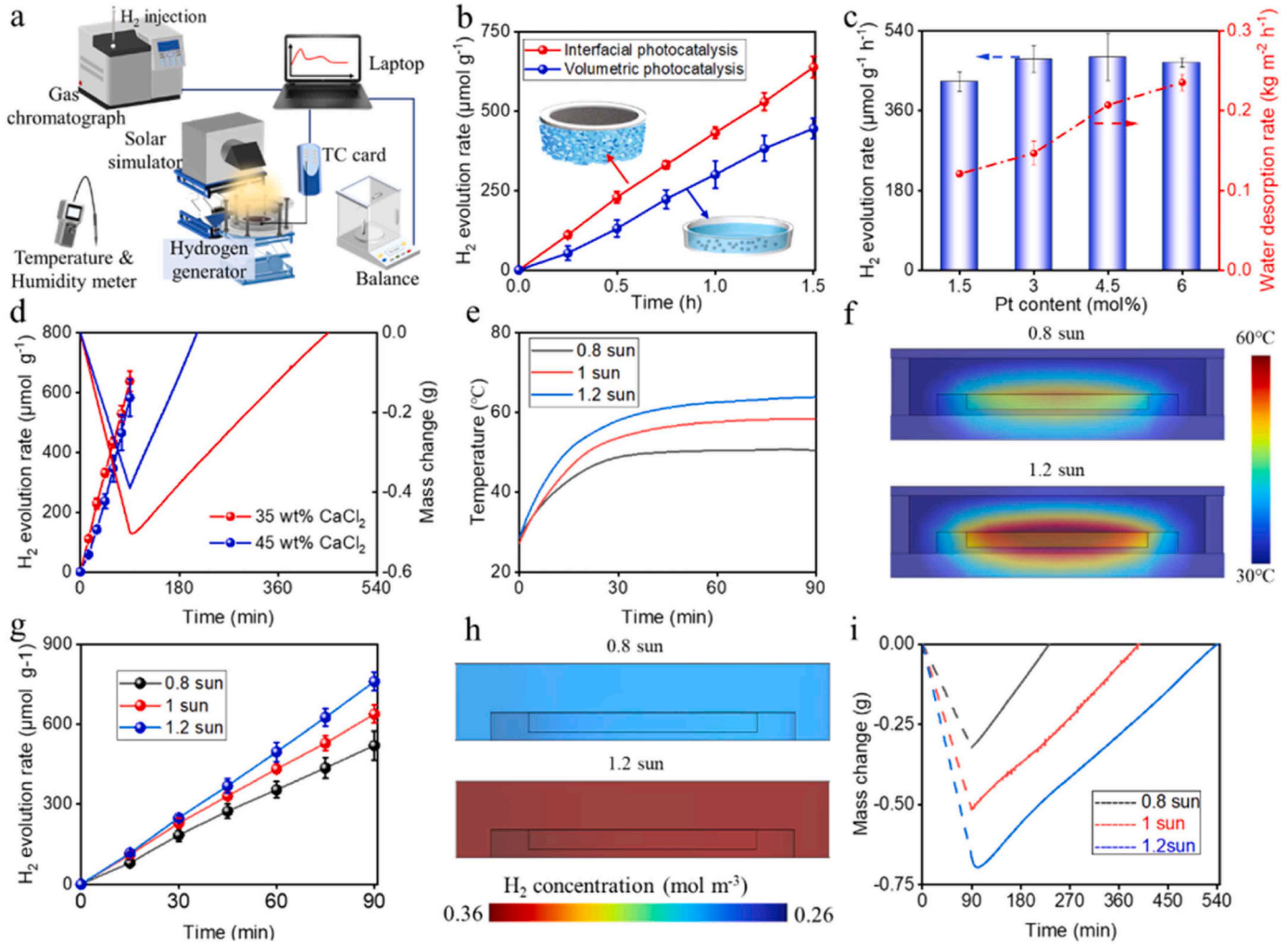

Fig. 3. Photocatalytic H_2 production and moisture harvesting performance evaluation of the AWH-PHE device in the laboratory under the ambient temperature of around 28 ℃ at ~70 % RH. a, Schematic of experimental setup consisting of an AWH-PHE device, a solar simulator, a gas chromatograph, a high precision balance, a temperature & humidity meter, and a PC. b, Comparison of hydrogen evolution performance between interfacial photocatalytic water vapor and volumetric photocatalysis in direct contact with bulk water under one sun illumination, and the corresponding physical picture is shown in Fig. S11. c, Water desorption rate and hydrogen production rate with different Pt content. d, Effects of different $CaCl_2$ content in hygroscopic hydrogel on H_2 production rate, water desorption and adsorption rates. e, Temperature evolution of the photocatalytic sheet under different solar intensities during a 1.5-hour test. f, Simulated temperature distribution under solar intensities of 0.8 and 1.2 sun for 1.5 hours. g, H_2 production varies with time under different solar intensities. h, Simulated H_2 concentration distribution under solar intensities of 0.8 sun and 1.2 sun for 1.5 hours. i, The mass change of water desorption process in hygroscopic hydrogel under different solar intensity and water vapor adsorption process in the dark.

as the ambient temperature increases from 16.4 °C to 45.6 °C. This is because as the ambient temperature increases, the reaction temperature of the whole device also increases, resulting in a larger water evaporation rate, and the larger partial pressure of water vapor around the photocatalytic layer will promote the photocatalytic reaction rate [38]. Moreover, a higher reaction temperature will reduce the diffusion resistance of H_2 gas [42], which will also accelerate the photocatalytic rate. Then, the hygroscopic dynamic characteristics of this device in the same dehydration state are evaluated under different environmental humidity (Fig. 4b). When the ambient humidity increases from 53 % to 85 %, the hygroscopic regeneration time of the $CaCl_2$-PAAm hydrogel decreases from 792 min to 197 min, which indicates that the $CaCl_2$ salt in the hygroscopic hydrogel has effective water vapor adsorption capacity in a wide range of humidity. Moreover, when the ambient humidity is lower than 45 %, the $CaCl_2$-PAAm hydrogel can still absorb moisture and realize self-regeneration (Fig. S16). To evaluate the working stability of this integrated device, five desorption hydrogen production and moisture absorption regeneration experiments are repeated under the ambient temperature of around 28 ℃ at 70 % RH - 75 % RH (Fig. 4c). The results indicate that there is no significant degradation in the overall performance of this device during cyclic operation, demonstrating satisfactory cycling stability. The excellent stability of the hybrid device is mainly attributed to the good vapor permeability and salt resistance of the hydrophobic PTFE film. Specifically, when the photocatalytic layer absorbs solar energy to heat the bottom hygroscopic hydrogel, the liquid water in the hydrogel underwent phase change to produce water vapor and diffuse to the surface of the catalyst through the hydrophobic film, while calcium ions are trapped at the interface between the hydrophobic film and the hydrogel, and cannot reach the photocatalytic layer, thus avoiding the pollution and damage of the catalyst by salts (Fig. 4d).

In order to confirm the salt resistance of the hydrophobic PTFE membrane, the distribution of elements on the surface of the photocatalytic layer is tested after several experiments, and the results show that Ti and Pt elements, which are the main components of the catalyst, still exist stably on the upper surface of the PTFE membrane, while the Ca element, which is the main component of the salt, does not appear on the upper surface after long-term operation. Moreover, the lower surface

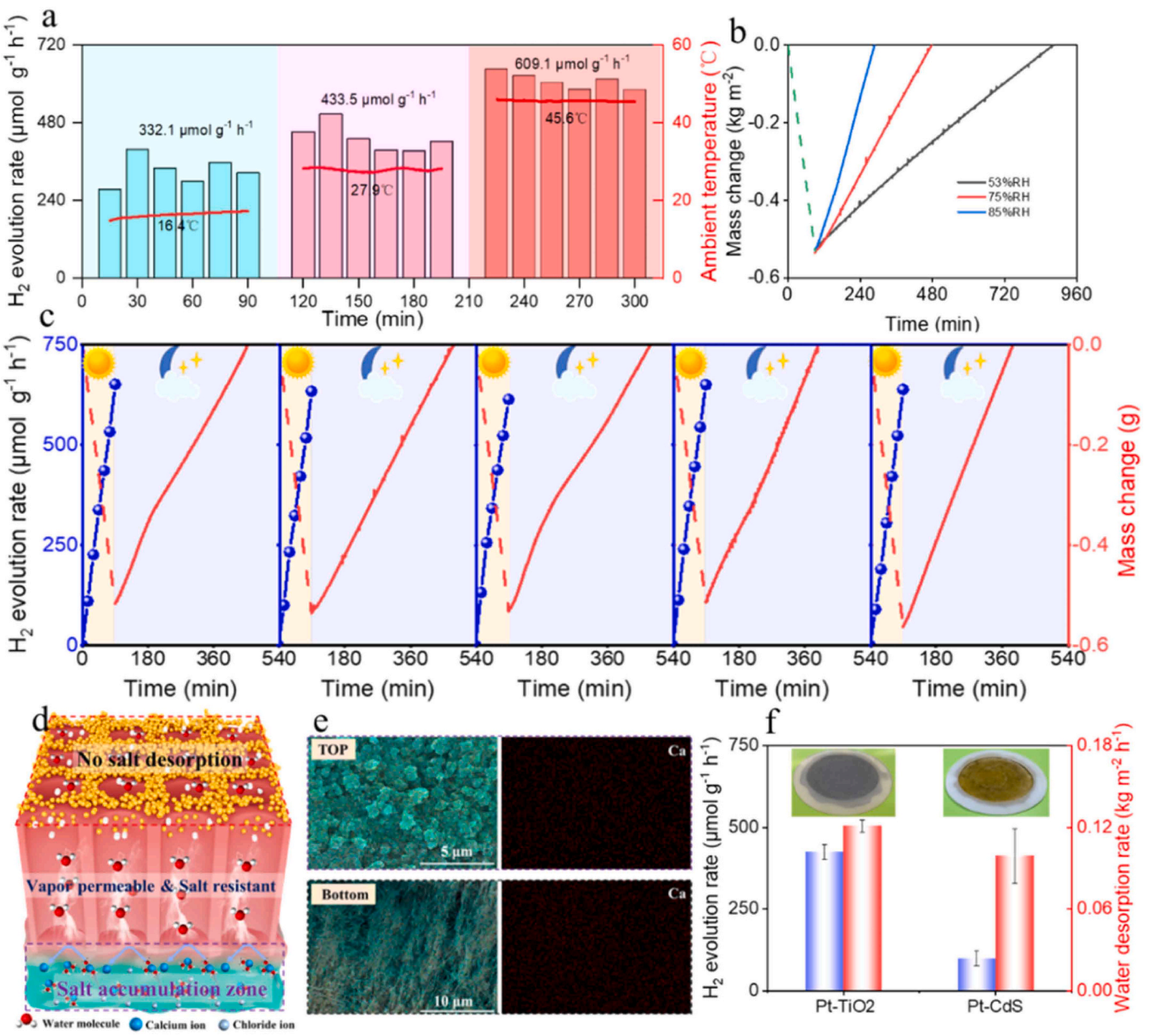

Fig. 4. Environment adaptability and operational stability of the AWH-PHE device. a, The H_2 production rate of the AWH-PHE device changes with time at different ambient temperatures under one sun illumination. b, Water vapor adsorption properties of the hygroscopic hydrogel (35 wt% $CaCl_2$) under average ambient humidity of 53 % RH, 75 % RH and 85 % RH. c, Five cycling tests of photocatalytic hydrogen production under one sun illumination and moisture harvesting regeneration in the AWH-PHE device. d, Schematic diagram of salt rejection mechanism in photocatalytic layer. e, The EDS mapping images of the top surface and bottom surface in photocatalytic layer after photocatalytic hydrogen production and moisture harvesting. f, The performance comparison between Pt-CdS catalyst and Pt-TiO_2 catalyst in this AWH-PHE system.

of PTFE film also does not adhere calcium salts due to its low surface energy (Fig. 4e). In addition, Fig. 4f and Fig. S17 show the performance comparison between Pt-CdS catalyst and Pt-TiO_2 catalyst in this AWH-PHE system. It can be seen that Pt-CdS catalyst achieves a hydrogen production rate of 98.63 μmol g^{-1} h^{-1} and a water desorption rate of 0.1 kg m^{-2} h^{-1}, indicating that this interfacial PHE system also has certain universality for different photocatalysts.

2.5. Outdoor performance evaluation

All previous experiments are conducted under controllable environmental conditions with constant solar intensity in the laboratory. However, the real outdoor weather conditions such as ambient temperature and relative humidity, solar intensity and wind velocity always fluctuate with time, which will inevitably affect the dynamic operation characteristics of the hybrid device. To demonstrate the feasibility of this integrated AWH-PHE device in the practical application, the outdoor experiments by using the same prototype as in the laboratory are performed on the rooftop of a building (Wuhan, China). Fig. 5a shows the layout of our outdoor experimental setup, in which the ambient temperature and relative humidity are recorded in real time using a temperature and humidity meter, and the change of sunlight intensity with time is collected in real time using a pyranometer. The amount of hydrogen produced by the device is collected once every hour by micro-injection needle and quantitatively calibrated by indoor gas chromatograph. The mass loss of the hygroscopic hydrogel during the desorption process and the real-time change in mass as it absorbs water vapor from the outdoor air are recorded by a precision balance. The 3D structure

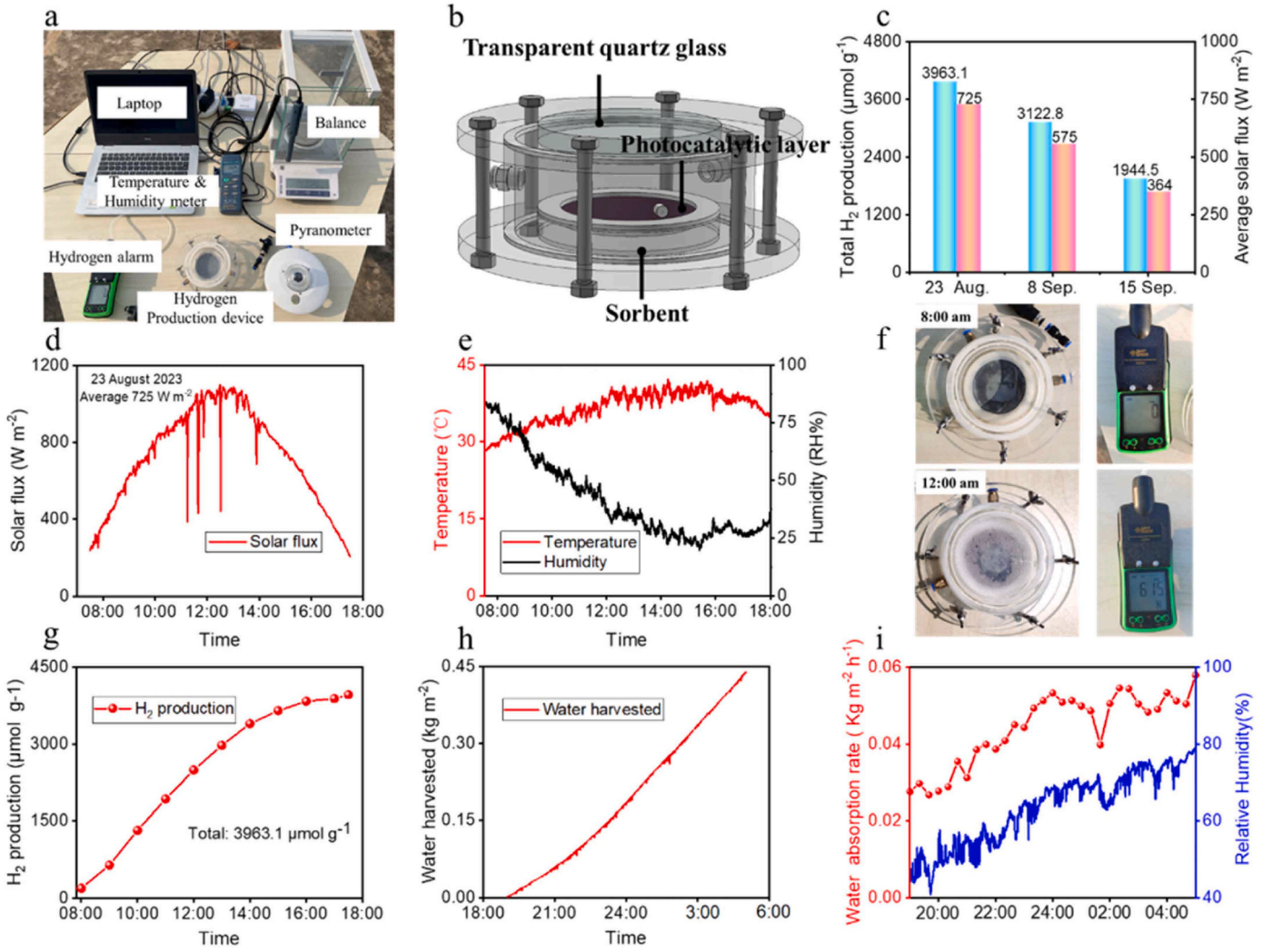

Fig. 5. H_2 production performance and water harvesting regeneration ability of the AWH-PHE prototype in real outdoor environment. a, The experimental setup on the rooftop, which consisted of a AWH-PHE prototype, a pyranometer, a high precision balance, a temperature & humidity meter, a hydrogen gas alarm and a laptop. b, 3D schematic diagram of the AWH-PHE prototype. c, Average daily solar intensity and total hydrogen production on different outdoor dates. d and e, Outdoor solar intensity, temperature and humidity changed over time on August 23th, 2023. f, The condensed water distribution inside the prototype and the hydrogen content value detected by the hydrogen gas alarm. g, The H_2 production of the prototype changed over time on August 23th, 2023. h and i, The outdoor water vapor adsorption performance of the device from the air at night and the relationship between the adsorption rate and environmental humidity.

diagram of the self-made AWH-PHE prototype is shown in Fig. 5b, in which the photocatalysis layer and hygroscopic hydrogel with a same effective area of 28.27 cm^2 are sealed in a closed acrylic chamber, and the upper layer is made of highly transparent quartz glass to avoid sunlight incident loss. Fig. 5c shows the daily average solar intensity and total hydrogen production on August 23th, September 8th and September 15th, which were 3963.1 μmol g^{-1} at 725 W m^{-2}, 3122.8 μmol g^{-1} at 575 W m^{-2} and 1944.5 μmol g^{-1} at 364 W m^{-2}, respectively. The variation trend of hydrogen production and outdoor solar intensity has a good consistency, which demonstrates the reliability of our integrated device in outdoor environment applications.

Taking the outdoor experiment that started on August 23th as an example (The results of September 8th and September 15th are shown in Fig. S18), during the daytime, the experiment started at 7:30 am and ended at 5:30 pm local time. The outdoor solar intensity, ambient temperature, and humidity were recorded over time on that day, with corresponding average values of 725 W m^{-2}, 36.7 °C, and 42.3 % RH (Fig. 5d and Fig. 5e). Fig. 5f shows the distribution of condensed water in the device and the internal hydrogen concentration value obtained by the hydrogen alarm. It can be seen that at 12:00 noon, the internal surface of the chamber was completely covered by condensed water and the hydrogen alarm detected obvious hydrogen components inside, indicating that the solar-driven desorption and photocatalytic water vapor process was reliable. During the 9.5-hour operation throughout the day, the prototype achieved a total hydrogen production of up to 3963.1 μmol g^{-1}, corresponding to a STH efficiency of 0.0859 % (Fig. 5g). At night, the prototype was opened and exposed to the outdoor environment, and began to capture water vapor from the ambient air. Fig. 5h shows the water vapor adsorption curve at that night. The hygroscopic regeneration process was completed from 7:00 p.m. to 5:00 a.m. the next day, and the adsorption rate of the hydrogel also showed good consistency with the change of environmental humidity (Fig. 5i), which indicated that the hygroscopic hydrogel prepared herein has good adsorption characteristics.

3. Conclusion

An integrated double-layer structure device is developed to spontaneously capture moisture from the air as a water source for in-situ photocatalytic hydrogen production. The Pt-TiO_2 photocatalytic layer in the device has a high absorption capacity in the whole solar spectrum, which ensures the synergistic effect of photocatalytic and photothermal.

In addition, the hydrophobic PTFE membrane was selected as the substrate of the photocatalytic layer due to its breathable and salt-resistant characteristics, thus the water vapor supply is ensured and the salt damage to the photocatalysis is effectively avoided. The prepared PAAm hydrogel with $CaCl_2$ salt has lower cost and good hygroscopic properties, which provides the possibility for large-scale promotion. As a result, the integrated AWH-PHE system can achieve a H_2 production rate of 425.4 μmol g^{-1} h^{-1} and a water desorption rate of 0.121 kg m^{-2} h^{-1} under one sun, and has a moisture adsorption rate of 0.03 kg m^{-2} h^{-1} under dark conditions in the laboratory. This system was also proven to possess good environmental adaptability and durability through multiple cycle experiments and variable operating conditions testing. Moreover, when the device is placed in real outdoor conditions, it obtains a total hydrogen production of up to 3963.1 μmol g^{-1} in the daytime and achieves water regeneration in the hygroscopic hydrogel within 10 hours by harvesting moisture from the surroundings at night, which confirms the feasibility of the system in practical application. The findings herein will introduce a promising route to produce green hydrogen fuel in remote arid areas with abundant solar energy.

4. Experimental section

4.1. Materials

Chloroplatinic acid hexahydrate ($H_2PtCl_6{\cdot}6\ H_2O$, analytical reagent, Pt ≥37.5 wt%), titanium dioxide, anatase (TiO_2, 60 nm, 99.8 %), acrylamide (AM, 99 %), and N, N`-methylenebis (acrylamide) (MBAA, 99 %) were purchased from Aladdin Biochemical Technology Co., Ltd. Calcium chloride ($CaCl_2$, analytical reagent), ethanol (C_2H_5OH, analytical reagent), ammonium persulfate (APS, analytical reagent), polyethylene glycol 2000 (PEG 2000, chemical reagent), and methanol (CH_3OH, analytical reagent) were purchased from Sinopharm Chemical Reagent Co., Ltd. Ultrahigh purity nitrogen (N_2, 99.999 %) was provided by Wuhan Xiangyun Industry and trade Co., Ltd. Deionized (DI) water, with a resistivity of 18.25 MΩ·cm, was produced and utilized throughout the experiments.

4.2. Synthesis of Pt/TiO_2 photocatalyst

Typically, the Pt/TiO_2 photocatalyst was obtained using the photodeposition method (Fig. S1). In detail, 1 g TiO_2 nanoparticles and 0.1 g $H_2PtCl_6{\cdot}6\ H_2O$ particles were dispersed in the glass beaker containing an aqueous solution of CH_3OH (30 mL, 10 vol%). Subsequently, the glass beaker was capsulated through a film of plastic wrap and placed on a magnetic stirrer (ZNCL-BS) with a speed of 1000 RPM, and the dispersed solution was irradiated under simulated solar irradiation (λ > 300 nm) provided by a xenon lamp (CEL-PE3^{00}L–^{3}A) for 2.5 h to adequately reduce the Pt ions, which an obvious color change of reaction solution from ivory to gray could be observed. In order to obtain the pure Pt/TiO_2 powder, the reacted solution was further purified through vacuum filtration procedure. In detail, the reacted solution was washed with DI water and C_2H_5OH solution alternately for several times through a vacuum pump (SHZ-D III), which equipped with a hydrophilic filter membrane (pore diameter: 0.2 μm), and Pt/TiO_2 solid powder was ultimately deposited on the filter membrane while unreacted impurities were removed. Then the pure Pt/TiO_2 photocatalyst powder with a Pt loading amount of 1.5 % was obtained after drying the moist Pt/TiO_2 mixture in the hot air circulating oven (101-OBS) with a temperature of 70 ℃ for 30 min.

4.3. Synthesis of $CaCl_2$-PAAm hydrogel

First, 2.843 g AM as monomer, 0.018 g MBAA as crosslinking agent, and 12.76 g $CaCl_2$ as a low-cost, environmentally friendly moisture adsorbent were uniformly dispersed in 20 mL DI water assisted by ultrasonication. Then the mixed solution was placed to cool down at room temperature with 25 ℃ for 15 min for avoiding instantly crosslinking. Subsequently, 0.052 g APS as thermal initiator was added into the mixed solution to form a homogeneous pre-polymer solution. The $CaCl_2$-PAAm hydrogel was obtained after pouring pre-polymer solution into a circular acrylic mould with a depth of 3 mm and a diameter of 60 mm, and polymerizing under ultraviolet illumination provided by a UV lamp for 25 min (Fig. S2).

4.4. Preparation of the AWH-PHE device

The prepared 70 mg $Pt\text{-}TiO_2$ photocatalyst powder was dispersed into ethanol aqueous solution (15 mL, 50 vol%), and then ultrasonic dispersed by an ultrasonic cell crusher for 30 minutes. The photocatalyst in ethanol aqueous solution was uniformly attached to the support layer of hydrophobic PTFE membrane (pore size 0.22 microns, thickness 120μm) with an effective diameter of 6 cm by vacuum filtration, and then the hydrophobic membrane with $Pt\text{-}TiO_2$ photocatalyst was dried in a 70 ℃ drying oven for 30 minutes. Subsequently, 1 mL PEG aqueous solution with a concentration of 50 mg mL^{-1} was dripped on the hydrophobic membrane as a sacrifice agent. After drying, it was cooled at room temperature to obtain a $Pt\text{-}TiO_2$ photocatalytic layer. Finally, the cooled photocatalytic layer was tightly bonded to the upper surface of the hygroscopic $CaCl_2$-PAAm hydrogel prepared in the acrylic mould by simple physical pressing (Fig. S3), and an AWH-PHE device with an effective area of 28.27 cm^2 was successfully obtained. The total cost of 1 m^2 AWH-PHE device was calculated and listed in Table S1 and Table S2.

4.5. Material characterization

SEM and EDS mapping images were obtained using a TESCAN MIRA3 field-emission scanning electron microscopy equipped with an Oxford Instruments Nanoanalysis Aztec Energy X-max 20 system. The absorption spectrum of the photocatalytic layer was characterized by a UV-Vis-NIR spectrophotometer (Shimadzu UV-3600). The contact angle of the samples was tested by a water contact angle measurement instrument (JC2000C, Shanghai). The temperature distribution of the AWH-PHE device was measured by an infrared thermal imager (FLIR E95).

4.6. Experimental measurement

In the photocatalytic hydrogen production experiment, both indoor and outdoor hydrogen evolution performance measurements were conducted in a 130 mL self-made sealed acrylic reaction chamber with a transparent quartz glass skylight (Fig. S7 and Fig. S8). Before the experiment, high-purity nitrogen gas was continuously introduced into the acrylic chamber for 10 minutes to eliminate the internal air. A 300 W solar simulator with AM 1.5 G standard optical filter (CEL-300 L-3A) was used to provide stable solar radiation and an optical power density meter (CEL-NP2000–2A) was used to calibrate the solar intensity. The hydrogen gas in the reaction chamber was sampled by a 1 mL micro injector at regular intervals and injected into a gas chromatograph (DJ-6890B, Fuli Insruments) for hydrogen content detection. The temperature of the photocatalytic layer was recorded in real time by a K-type thermocouple (TT-K-30-SLE) connected to a temperature acquisition card (TC-08). The temperature and relative humidity were obtained by a Temperature & Humidity meter (CENTER 313). A precision electronic balance (ME-204, METTLER TOLEDO) was used to weigh the water loss of hygroscopic hydrogels during solar-driven desorption process and to record real-time mass change of moisture absorption from the environment at night or in the dark. In outdoor experiments, a thermoelectric solar intensity meter (RENKE RS-TBQ-NO1-AL) was used to record the solar flux over time. A hydrogen alarm (AS8909) was used to visually and qualitatively obtain the hydrogen content in the reaction chamber.

CRediT authorship contribution statement

Xiantao Zhang: Software, Investigation, Formal analysis, Data curation. **Chengxiang Gui:** Software, Formal analysis, Data curation. **Tingting Ren:** Methodology, Investigation, Formal analysis. **Lu Huang:** Writing – original draft, Investigation, Funding acquisition, Conceptualization. **Chenglong Qin:** Software, Investigation, Formal analysis, Data curation. **Peng Liu:** Writing – original draft, Methodology, Investigation, Funding acquisition, Conceptualization. **Yingni Yu:** Methodology, Investigation, Formal analysis. **Yanlin Ge:** Methodology, Investigation, Formal analysis. **Lingen Chen:** Writing – review & editing, Supervision, Funding acquisition, Conceptualization. **Zhichun Liu:** Supervision, Conceptualization.

Declaration of Competing Interest

The authors declare that they have no known competing financial interests or personal relationships that could have appeared to influence the work reported in this paper.

Data Availability

No data was used for the research described in the article.

Acknowledgements

This work acknowledges funding support from the National Natural Science Foundation of China (Nos. 52306110, 52171317 and 52206108), and the Natural Science Foundation of Hubei Province (Nos. 2023AFB078 and 2022CFB677). The authors wish to thank the editor and reviewers for their careful, unbiased and constructive suggestions, which led to this revised manuscript.

Appendix A. Supporting information

Supplementary data associated with this article can be found in the online version at doi:10.1016/j.nanoen.2024.109879.

References

[1] D. Tonelli, L. Rosa, P. Gabrielli, K. Caldeira, A. Parente, F. Contino, Global land and water limits to electrolytic hydrogen production using wind and solar resources, Nat. Commun. 14 (2023) 5532, https://doi.org/10.1038/s41467-023-41107-x.
[2] Y. Zhang, J. Zhao, H. Wang, B. Xiao, W. Zhang, X. Zhao, T. Lv, M. Thangamuthu, J. Zhang, Y. Guo, J. Ma, L. Lin, J. Tang, R. Huang, Q. Liu, Single-atom Cu anchored catalysts for photocatalytic renewable H2 production with a quantum efficiency of 56%, Nat. Commun. 13 (2022) 58, https://doi.org/10.1038/s41467-021-27698-3.
[3] J. Guo, Y. Zhang, A. Zavabeti, K. Chen, Y. Guo, G. Hu, X. Fan, G.K. Li, Hydrogen production from the air, Nat. Commun. 13 (2022) 5046, https://doi.org/10.1038/s41467-022-32652-y.
[4] Y. Zhang, Y. Li, X. Xin, Y. Wang, P. Guo, R. Wang, B. Wang, W. Huang, A. J. Sobrido, X. Li, Internal quantum efficiency higher than 100% achieved by combining doping and quantum effects for photocatalytic overall water splitting, Nat. Energy 8 (2023) 504–514, https://doi.org/10.1038/s41560-023-01242-7.
[5] X. Wang, L. Chen, S.Y. Chong, M.A. Little, Y. Wu, W.-H. Zhu, R. Clowes, Y. Yan, M. A. Zwijnenburg, R.S. Sprick, A.I. Cooper, Sulfone-containing covalent organic frameworks for photocatalytic hydrogen evolution from water, Nat. Chem. 10 (2018) 1180–1189, https://doi.org/10.1038/s41557-018-0141-5.
[6] D. Zhao, Y. Wang, C.-L. Dong, Y.-C. Huang, J. Chen, F. Xue, S. Shen, L. Guo, Boron-doped nitrogen-deficient carbon nitride-based Z-scheme heterostructures for photocatalytic overall water splitting, Nat. Energy 6 (2021) 388–397, https://doi.org/10.1038/s41560-021-00795-9.
[7] P. Varadhan, H.-C. Fu, Y.-C. Kao, R.-H. Horng, J.-H. He, An efficient and stable photoelectrochemical system with 9% solar-to-hydrogen conversion efficiency via InGaP/GaAs double junction, Nat. Commun. 10 (2019) 5282, https://doi.org/10.1038/s41467-019-12977-x.
[8] J. Jia, L.C. Seitz, J.D. Benck, Y. Huo, Y. Chen, J.W.D. Ng, T. Bilir, J.S. Harris, T. F. Jaramillo, Solar water splitting by photovoltaic-electrolysis with a solar-to-hydrogen efficiency over 30, Nat. Commun. 7 (2016) 13237, https://doi.org/10.1038/ncomms13237.
[9] Y. Goto, T. Hisatomi, Q. Wang, T. Higashi, K. Ishikiriyama, T. Maeda, Y. Sakata, S. Okunaka, H. Tokudome, M. Katayama, S. Akiyama, H. Nishiyama, Y. Inoue, T. Takewaki, T. Setoyama, T. Minegishi, T. Takata, T. Yamada, K. Domen, A particulate photocatalyst water-splitting panel for large-scale solar hydrogen generation, Joule 2 (2018) 509–520, https://doi.org/10.1016/j.joule.2017.12.009.
[10] S. Chen, T. Takata, K. Domen, Particulate photocatalysts for overall water splitting, Nat. Rev. Mater. 2 (2017) 17050, https://doi.org/10.1038/natrevmats.2017.50.
[11] H. Nishiyama, T. Yamada, M. Nakabayashi, Y. Maehara, M. Yamaguchi, Y. Kuromiya, Y. Nagatsuma, H. Tokudome, S. Akiyama, T. Watanabe, R. Narushima, S. Okunaka, N. Shibata, T. Takata, T. Hisatomi, K. Domen, Photocatalytic solar hydrogen production from water on a 100-m^2 scale, Nature 598 (2021) 304–307, https://doi.org/10.1038/s41586-021-03907-3.
[12] C.-Z. Ning, L. Dou, P. Yang, Bandgap engineering in semiconductor alloy nanomaterials with widely tunable compositions, Nat. Rev. Mater. 2 (2017) 17070, https://doi.org/10.1038/natrevmats.2017.70.
[13] L. Guo, Z. Yang, K. Marcus, Z. Li, B. Luo, L. Zhou, X. Wang, Y. Du, Y. Yang, MoS_2/TiO_2 heterostructures as nonmetal plasmonic photocatalysts for highly efficient hydrogen evolution, Energ. Environ. Sci. 11 (2018) 106–114, https://doi.org/10.1039/c7ee02464a.
[14] R. Li, H. Han, F. Zhang, D. Wang, C. Li, Highly efficient photocatalysts constructed by rational assembly of dual-cocatalysts separately on different facets of $BiVO_4$, Energ. Environ. Sci. 7 (2014) 1369, https://doi.org/10.1039/c3ee43304h.
[15] X. Tao, Y. Zhao, S. Wang, C. Li, R. Li, Recent advances and perspectives for solar-driven water splitting using particulate photocatalysts, Chem. Soc. Rev. 51 (2022) 3561–3608, https://doi.org/10.1039/d2cs90098j.
[16] P. Zhou, I.A. Navid, Y. Ma, Y. Xiao, P. Wang, Z. Ye, B. Zhou, K. Sun, Z. Mi, Solar-to-hydrogen efficiency of more than 9% in photocatalytic water splitting, Nature 613 (2023) 66–70, https://doi.org/10.1038/s41586-022-05399-1.
[17] M. Gao, P.K.N. Connor, G.W. Ho, Plasmonic photothermic directed broadband sunlight harnessing for seawater catalysis and desalination, Energ. Environ. Sci. 9 (2016) 3151–3160, https://doi.org/10.1039/c6ee00971a.
[18] S. Fang, X. Lyu, T. Tong, A.I. Lim, T. Li, J. Bao, Y.H. Hu, Turning dead leaves into an active multifunctional material as evaporator, photocatalyst, and bioplastic, Nat. Commun. 14 (2023) 1203, https://doi.org/10.1038/s41467-023-36783-8.
[19] W.H. Lee, C.W. Lee, G.D. Cha, B.-H. Lee, J.H. Jeong, H. Park, J. Heo, M. S. Bootharaju, S.-H. Sunwoo, J.H. Kim, K.H. Ahn, D.-H. Kim, T. Hyeon, Floatable photocatalytic hydrogel nanocomposites for large-scale solar hydrogen production, Nat. Nanotechnol. 18 (2023) 754–762, https://doi.org/10.1038/s41565-023-01385-4.
[20] A.K. Rao, A.J. Fix, Y.C. Yang, D.M. Warsinger, Thermodynamic limits of atmospheric water harvesting, Energ. Environ. Sci. 15 (2022) 4025–4037, https://doi.org/10.1039/d2ee01071b.
[21] H. Shan, P. Poredoš, Z. Ye, H. Qu, Y. Zhang, M. Zhou, R. Wang, S.C. Tan, All-day multicyclic atmospheric water harvesting enabled by polyelectrolyte hydrogel with hybrid desorption mode, Adv. Mater. 35 (2023) 2302038, https://doi.org/10.1002/adma.202302038.
[22] M. Ejeian, R.Z. Wang, Adsorption-based atmospheric water harvesting, Joule 5 (2021) 1678–1703, https://doi.org/10.1016/j.joule.2021.04.005.
[23] S. Gao, Y. Wang, C. Zhang, M. Jiang, S. Wang, Z. Wang, Tailoring interfaces for atmospheric water harvesting: Fundamentals and applications, Matter 6 (2023) 2182–2205, https://doi.org/10.1016/j.matt.2023.04.008.
[24] R. Ghosh, A. Baut, G. Belleri, M. Kappl, H.-J. Butt, T.M. Schutzius, Photocatalytically reactive surfaces for simultaneous water harvesting and treatment, Nat. Sustain. 6 (2023) 1663–1672, https://doi.org/10.1038/s41893-023-01159-9.
[25] J. Xu, T. Li, T. Yan, S. Wu, M. Wu, J. Chao, X. Huo, P. Wang, R. Wang, Ultrahigh solar-driven atmospheric water production enabled by scalable rapid-cycling water harvester with vertically aligned nanocomposite sorbent, Energ. Environ. Sci. 14 (2021) 5979–5994, https://doi.org/10.1039/d1ee01723c.
[26] J. Wang, L. Hua, C. Li, R. Wang, Atmospheric water harvesting: critical metrics and challenges, Energ. Environ. Sci. 15 (2022) 4867–4871, https://doi.org/10.1039/d2ee03079a.
[27] R. Li, P. Wang, Sorbents, processes and applications beyond water production in sorption-based atmospheric water harvesting, Nat. Water 1 (2023) 573–586, https://doi.org/10.1038/s44221-023-00099-0.
[28] T. Li, M. Wu, J. Xu, R. Du, T. Yan, P. Wang, Z. Bai, R. Wang, S. Wang, Simultaneous atmospheric water production and 24-hour power generation enabled by moisture-induced energy harvesting, Nat. Commun. 13 (2022) 6771, https://doi.org/10.1038/s41467-022-34385-4.
[29] N. Hanikel, X. Pei, S. Chheda, H. Lyu, W. Jeong, J. Sauer, L. Gagliardi, O.M. Yaghi, Evolution of water structures in metal-organic frameworks for improved atmospheric water harvesting, Science 374 (2021) 454–459, https://doi.org/10.1126/science.abj0890.
[30] H. Kim, S. Yang, S.R. Rao, S. Narayanan, E.A. Kapustin, H. Furukawa, A.S. Umans, O.M. Yaghi, E.N. Wang, Water harvesting from air with metal-organic frameworks powered by natural sunlight, Science 356 (2017) 430–434, https://doi.org/10.1126/science.aam8743.
[31] A. LaPotin, Y. Zhong, L. Zhang, L. Zhao, A. Leroy, H. Kim, S.R. Rao, E.N. Wang, Dual-stage atmospheric water harvesting device for scalable solar-driven water production, Joule 5 (2021) 166–182, https://doi.org/10.1016/j.joule.2020.09.008.
[32] S.H. Nah, Y. Lee, K.H. Yu, Y. Chi, H. Lee, B. Chen, M. Patel, K. Wang, S. Yang, Moisture absorbing and water self-releasing from hybrid hydrogel desiccants, Adv. Funct. Mater. (2023) 2313881, https://doi.org/10.1002/adfm.202470105.
[33] R. Li, Y. Shi, M. Wu, S. Hong, P. Wang, Photovoltaic panel cooling by atmospheric water sorption-evaporation cycle, Nat. Sustain. 3 (2020) 636–643, https://doi.org/10.1038/s41893-020-0535-4.

[34] C. Lei, Y. Guo, W. Guan, H. Lu, W. Shi, G. Yu, Polyzwitterionic hydrogels for efficient atmospheric water harvesting, Angew. Chem. Int. Ed. 61 (2022) e202200271, https://doi.org/10.1002/anie.202200271.
[35] J. Lord, A. Thomas, N. Treat, M. Forkin, R. Bain, P. Dulac, C.H. Behroozi, T. Mamutov, J. Fongheiser, N. Kobilansky, S. Washburn, C. Truesdell, C. Lee, P. H. Schmaelzle, Global potential for harvesting drinking water from air using solar energy, Nature 598 (2021) 611–617, https://doi.org/10.1038/s41586-021-03900-w.
[36] Y. Wang, W. Zhao, M. Han, J. Xu, K.C. Tam, Biomimetic surface engineering for sustainable water harvesting systems, Nat. Water 1 (2023) 587–601, https://doi.org/10.1038/s44221-023-00109-1.
[37] Y. Song, N. Xu, G. Liu, H. Qi, W. Zhao, B. Zhu, L. Zhou, J. Zhu, High-yield solar-driven atmospheric water harvesting of metal-organic-framework-derived nanoporous carbon with fast-diffusion water channels, Nat. Nanotechnol. 17 (2022) 857–863, https://doi.org/10.1038/s41565-022-01135-y.
[38] C. Pornrungroj, A.B. Mohamad Annuar, Q. Wang, M. Rahaman, S. Bhattacharjee, V. Andrei, E. Reisner, Hybrid photothermal-photocatalyst sheets for solar-driven overall water splitting coupled to water purification, Nat. Water 1 (2023) 952–960, https://doi.org/10.1038/s44221-023-00139-9.
[39] Y. Liu, W.-K. Han, W. Chi, J.-X. Fu, Y. Mao, X. Yan, J.-X. Shao, Y. Jiang, Z.-G. Gu, One-dimensional covalent organic frameworks with atmospheric water harvesting for photocatalytic hydrogen evolution from water vapor, Appl. Catal. B-Environ. 338 (2023) 123074, https://doi.org/10.1016/j.apcatb.2023.123074.
[40] L. He, X. Zeng, H. Chen, L. Zhao, Z. Huang, D. Wang, X. He, W. Fang, X. Du, W. Li, A hybrid photocatalytic system splits atmospheric water to produce hydrogen, Adv. Funct. Mater. (2024), https://doi.org/10.1002/adfm.202313058.
[41] Q. Cheng, Y. Yuan, R. Tang, Q. Liu, L. Bao, P. Wang, J. Zhong, Z. Zhao, Z. Yu, Z. Zou, Rapid hydroxyl radical generation on (001)-facet-exposed ultrathin anatase TiO_2 nanosheets for enhanced photocatalytic lignocellulose-to-H_2 conversion, ACS Catal. 12 (2022) 2118–2125, https://doi.org/10.1021/acscatal.1c05713.
[42] S. Guo, X. Li, J. Li, B. Wei, Boosting photocatalytic hydrogen production from water by photothermally induced biphase systems, Nat. Commun. 12 (2021) 1343, https://doi.org/10.1038/s41467-021-21526-4.

Dr. Lu Huang received her Ph.D. in Engineering thermophysics from Wuhan University in 2021, under the supervision of Prof. Xuejiao Hu. He joined the School of Mechanical and Electrical Engineering, Wuhan Institute of Technology (WIT) as a research scientist in 2021. His research focuses on solar-driven hydrogen production, solar desalination, electronic cooling, thermo-osmotic energy conversion.

Prof. Peng Liu received his Ph.D. in Engineering thermophysics from Huazhong University of Science and Technology (HUST) in 2019, under the supervision of Prof. Wei Liu. After that he joint Wei Liu's group as a postdoctoral research fellow. He joined the School of Mechanical and Electrical Engineering, Wuhan Institute of Technology (WIT) as an associate professor in 2021. His research focuses on heat and mass transfer enhancement theory and technology, solar driven hydrogen production, electronic cooling, solar collector and thermal energy storage.

Chenglong Qin received his B.S. degree Wuhan Institute of Technology in 2022. Currently, he is a master candidate in the School of Mechanical and Electrical Engineering, Wuhan Institute of Technology, under the supervision of Dr. Lu Huang. His main research interest is advanced photocatalytic system.

Chengxiang Gui received his B.S. degree from Henan University of Science and Technology in 2021. Currently, he is a graduate student in the School of Mechanical and Electrical Engineering of Wuhan Institute of Technology, under the supervision of Dr. Lu Huang. His current research interests focus on efficient utilization of renewable energy, and packaging of multi-effect hybrid systems.

Dr. Zhang Xiantao received the Ph.D. in Thermal Energy from Wuhan University in 2017. After that, he worked as a researcher at Wuhan Institute of Technology, and current research interest focuses on the efficient utilization of waste heat.

Dr. Tingting Ren received her Ph.D. in Nuclear Science and Technology from Harbin Engineering University in 2021. After that, she worked as a researcher at Wuhan Institute of Technology. Her current research interest focuses on the flow and heat transfer in Micronano channel and bubble dynamics.

Prof. Yanlin Ge received his Ph.D. in power engineering and engineering thermophysics from the Naval University of Engineering, P R China in 2011, under the supervision of Prof. Lingen Chen. After that he joined the Naval University of Engineering and he was promoted to associate professor in 2014. and now he is a full professor in Wuhan Institute of Technology. His research focuses the topic in Finite Time Thermodynamics (or Entropy Generation Minimization, or Thermodynamic Optimization). He is the author or co-author of over 350 peer-refereed articles (over 170 in English journals) and 1 book.

Dr. Yingni Yu received her Ph.D. in Thermal Energy from Huazhong University of Science and Technology in 2022. After that, she worked as a researcher at Wuhan Institute of Technology. Her current research interest focuses on the synthesis of nanomaterials and nanostructures for advanced catalysis applications such as water splitting for hydrogen and oxygen evolution, CO_2 reduction reactions and utilization of solid waste.

Prof. Zhichun Liu received his Ph.D. from the School of Energy and Power Engineering, Huazhong University of Science and Technology of China (HUST) in 2006, and was visiting scholar in Massachusetts Institute of Technology, US in 2012. Since 2014, he is a professor in the School of Energy and Power Engineering, HUST. His research focuses on heat and mass transfer in nanoscale and photocatalysis system, electronic cooling, porous media and energy conservation. He has published more than 100 academic papers included in SCI.

Prof. Lingen Chen joined the Chinese Navy in 1979 and received his Ph.D. in power engineering and engineering thermophysics from the Naval University of Engineering, P R China in 1998. He joined the Naval University of Engineering as research scientist in 1986 and he was promoted to professor in 1996. Now, he is the Director of the Institute of Thermal Science and Power Engineering, Wuhan Institute of Technology, P R China. His research focuses on Finite Time Thermodynamics, Quantum Thermodynamics, Constructal Theory, Optimal Design et. al. He is the author or co-author of over 2140 peer-refereed articles and 20 books.